

Segmented Band Mechanism for Itinerant Ferromagnetism

C. D. Batista,¹ J. Bonča,² and J. E. Gubernatis¹

¹Center for Nonlinear Studies and Theoretical Division Los Alamos National Laboratory, Los Alamos, NM 87545

²Department of Physics, FMF, University of Ljubljana and J. Stefan Institute, Ljubljana, Slovenia
(February 1, 2008)

We introduce a novel mechanism for itinerant ferromagnetism, which is based on a simple two-band model, and using numerical and analytical methods, we show that the Periodic Anderson Model (PAM) contains this mechanism. We propose that the mechanism, which does not assume an intra-atomic Hund's coupling, is present in both the iron group and some f electron compounds.

Even though itinerant ferromagnetism was the first collective electronic phenomena studied quantum mechanically, the microscopic mechanisms driving this phase are still unknown [1,2]. In 1928, Heisenberg [3] formulated his spin model to address this issue, but as Bloch [4] pointed out, a model of localized spins cannot explain the metallic ferromagnetism observed in Fe, Co and Ni. After seven decades of intense effort we still do not know what is the minimal model of itinerant ferromagnetism and, more importantly, the basic mechanism of ordering.

In 1963, Hubbard [5] and others introduced the Hubbard model to explain the ferromagnetic (FM) properties of the iron group, incorporating the kinetic energy in a *single nondegenerate band* with an intra-atomic Coulomb repulsion U . With the exception of Nagaoka's [6] and Lieb's [7] theorems, subsequent theoretical approaches were not controlled enough to determine whether the Hubbard model has a FM phase. The central issue is the precise evaluation of the energy for the paramagnetic (PM) phase. Because it does not properly incorporate the correlations, mean field theory overestimates this energy and predicts a large FM region [1]. In contrast, numerical calculations have narrowed the extent of this phase to a small region around the Nagaoka point [6].

Going beyond the simple one-band Hubbard model is advocated, for example, by Vollhardt et. al. [1]. They note that the inclusion of additional density-density interactions, correlated hoppings, and direct exchange terms favors FM ordering. A very simple analysis shows that increasing the density of states $\mathcal{D}(E)$ below the Fermi energy E_F and placing E_F close to the lower band edge increases the FM tendency. One can achieve this by including additional hopping terms. The effectiveness of a next nearestneighbor hopping t' was studied numerically by Hlubina *et al* [8] for the Hubbard model on a square lattice. They found a FM state when the van Hove singularity in $\mathcal{D}(E)$ occurred at E_F . However, this phase was not robust against very small changes in t' .

Years ago, Slater [9] and van Vleck [10] speculated that band degeneracy is an essential precondition for itinerant ferromagnetism. They suggested that the intra-atomic Hund coupling in open shells could be transmitted from one atom to another by the conduction electrons.

However, there are FM metals like Ni where the influence of the Hund's coupling is not clear. In Ni, Hund's coupling is associated with the $3d^8$ configuration which has low probability as the main configurations are roughly 40% of $3d^{10}$ and 60% of $3d^9$ [10]. The relevant question for some transition metals is thus whether a model involving just the two configurations is sufficient, or are other orbitals and Hund's exchange necessary to explain ferromagnetism. Furthermore, there are f electron itinerant ferromagnets, like CeRh_3B_2 [11], whose only local magnetic coupling is Kondo like, i.e. antiferromagnetic.

The novel mechanism we now introduce emerges from a two-band model, such as the periodic Anderson model (PAM). The basic ingredients are an uncorrelated dispersive band hybridized with a correlated and narrow band. Missing is an explicit intra-atomic Hund's exchange. We show the PAM supports our mechanism by interpreting the results of quantum Monte Carlo (QMC) simulations with an effective model derived from it.

We will discuss our mechanism in the context of:

$$H = -t_b \sum_{\langle \mathbf{r}, \mathbf{r}' \rangle, \sigma} (b_{\mathbf{r}\sigma}^\dagger b_{\mathbf{r}'\sigma} + b_{\mathbf{r}'\sigma}^\dagger b_{\mathbf{r}\sigma}) + V \sum_{\mathbf{r}, \sigma} (b_{\mathbf{r}\sigma}^\dagger a_{\mathbf{r}\sigma} + a_{\mathbf{r}\sigma}^\dagger b_{\mathbf{r}\sigma}) - t_a \sum_{\langle \mathbf{r}, \mathbf{r}' \rangle, \sigma} (a_{\mathbf{r}\sigma}^\dagger a_{\mathbf{r}'\sigma} + a_{\mathbf{r}'\sigma}^\dagger a_{\mathbf{r}\sigma}) + \epsilon_a \sum_{\mathbf{r}, \sigma} n_{\mathbf{r}\sigma}^a + \frac{U}{2} \sum_{\mathbf{r}, \sigma} n_{\mathbf{r}\sigma}^a n_{\mathbf{r}\bar{\sigma}}^a,$$

where $b_{\mathbf{r}\sigma}^\dagger$ and $a_{\mathbf{r}\sigma}^\dagger$ create an electron with spin σ in b and a orbitals at lattice site \mathbf{r} and $n_{\mathbf{r}\sigma}^a = a_{\mathbf{r}\sigma}^\dagger a_{\mathbf{r}\sigma}$. The t_b and t_a hoppings are only to nearest-neighbor sites. When $t_a = 0$, the Hamiltonian is the standard PAM. For the f electron compounds, the a and b orbitals play the role of the f and d orbitals, and $t_a \approx 0$. For transition metals, they correspond to the $3d$ and $4s$ orbitals. For $U = 0$, the resulting Hamiltonian H_0 is easily diagonalized:

$$H_0 = \sum_{\mathbf{k}, \sigma} \left(E_{\mathbf{k}}^+ \beta_{\mathbf{k}\sigma}^\dagger \beta_{\mathbf{k}\sigma} + E_{\mathbf{k}}^- \alpha_{\mathbf{k}\sigma}^\dagger \alpha_{\mathbf{k}\sigma} \right) \\ E_{\mathbf{k}}^\pm = \frac{1}{2} \left[e_{\mathbf{k}}^b + e_{\mathbf{k}}^a \pm \sqrt{(e_{\mathbf{k}}^b - e_{\mathbf{k}}^a)^2 + 4V^2} \right] \quad (1)$$

with $e_{\mathbf{k}}^b = -2t_b \sum_{i=1}^D \cos k_{x_i}$ and $e_{\mathbf{k}}^a = \epsilon_a - 2t_a \sum_{i=1}^D \cos k_{x_i}$ for a hypercubic lattice in dimension D .

The operators which create quasi-particles in the lower and upper bands are:

$$\alpha_{\mathbf{k}\sigma}^\dagger = u_{\mathbf{k}} a_{\mathbf{k}\sigma}^\dagger + v_{\mathbf{k}} b_{\mathbf{k}\sigma}^\dagger, \quad \beta_{\mathbf{k}\sigma}^\dagger = -v_{\mathbf{k}} a_{\mathbf{k}\sigma}^\dagger + u_{\mathbf{k}} b_{\mathbf{k}\sigma}^\dagger$$

$$u_{\mathbf{k}} = \frac{E_{\mathbf{k}}^+ - e_{\mathbf{k}}^a}{\sqrt{(E_{\mathbf{k}}^+ - e_{\mathbf{k}}^a)^2 + V^2}}, \quad v_{\mathbf{k}} = \frac{-V}{\sqrt{(E_{\mathbf{k}}^+ - e_{\mathbf{k}}^a)^2 + V^2}}. \quad (2)$$

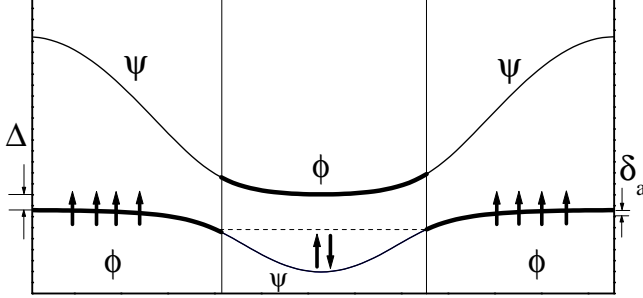


FIG. 1. Illustration of the effective model and the FM mechanism. Δ is the hybridization gap and δ_a is the interval of energy where the electrons are polarized.

In Fig. 1, we illustrate the (one-dimensional) non-interacting bands for the case of interest: ϵ_a close to E_F and above the bottom of the b band. If $|V| \ll |t_b|$, we can identify two subspaces in each band where the states have either predominantly b (ψ subspace) or a (ϕ subspace) character. The size of the crossover region around the points where the original unhybridized b and a bands crossed is proportional to $|V/t_b|$; that is, it is very small. The creation operators for the Wannier orbitals $\psi_{\mathbf{r}\sigma}$ and $\phi_{\mathbf{r}\sigma}$ associated with each subspace are:

$$\psi_{\mathbf{r}\sigma}^\dagger = \frac{1}{\sqrt{N}} \left[\sum_{\mathbf{k} \in \mathbf{K}^>} e^{i\mathbf{k} \cdot \mathbf{r}} \beta_{\mathbf{k}\sigma}^\dagger + \sum_{\mathbf{k} \in \mathbf{K}^<} e^{i\mathbf{k} \cdot \mathbf{r}} \alpha_{\mathbf{k}\sigma}^\dagger \right]$$

$$\phi_{\mathbf{r}\sigma}^\dagger = \frac{1}{\sqrt{N}} \left[\sum_{\mathbf{k} \in \mathbf{K}^>} e^{i\mathbf{k} \cdot \mathbf{r}} \alpha_{\mathbf{k}\sigma}^\dagger + \sum_{\mathbf{k} \in \mathbf{K}^<} e^{i\mathbf{k} \cdot \mathbf{r}} \beta_{\mathbf{k}\sigma}^\dagger \right]. \quad (3)$$

where N is the number of sites. The subsets $\mathbf{K}^>$ and $\mathbf{K}^<$ are defined by: $\mathbf{K}^> = \{\mathbf{k} : |u_{\mathbf{k}}| \geq |v_{\mathbf{k}}|\}$ and $\mathbf{K}^< = \{\mathbf{k} : |v_{\mathbf{k}}| > |u_{\mathbf{k}}|\}$. In this new basis:

$$H_0 = H_0^\phi + H_0^\psi = \sum_{\mathbf{r}, \mathbf{r}', \sigma} \tau_{\mathbf{r}-\mathbf{r}'}^\phi \phi_{\mathbf{r}\sigma}^\dagger \phi_{\mathbf{r}'\sigma} + \sum_{\mathbf{r}, \mathbf{r}', \sigma} \tau_{\mathbf{r}-\mathbf{r}'}^\psi \psi_{\mathbf{r}\sigma}^\dagger \psi_{\mathbf{r}'\sigma},$$

with $\tau_{\mathbf{r}}^\phi = \frac{1}{N} [\sum_{\mathbf{k} \in \mathbf{K}^>} e^{i\mathbf{k} \cdot \mathbf{r}} E_{\mathbf{k}}^- + \sum_{\mathbf{k} \in \mathbf{K}^<} e^{i\mathbf{k} \cdot \mathbf{r}} E_{\mathbf{k}}^+]$ and $\tau_{\mathbf{r}}^\psi = \frac{1}{N} [\sum_{\mathbf{k} \in \mathbf{K}^>} e^{i\mathbf{k} \cdot \mathbf{r}} E_{\mathbf{k}}^+ + \sum_{\mathbf{k} \in \mathbf{K}^<} e^{i\mathbf{k} \cdot \mathbf{r}} E_{\mathbf{k}}^-]$.

Because the U term in H involves only the a orbitals, the matrix elements of H connecting the ϕ and ψ subspaces are small compared to the characteristic energy scales of the problem (the matrix elements of H within the subspaces). To see this we express $a_{\mathbf{r}\sigma}^\dagger$ as a function of $\phi_{\mathbf{r}\sigma}^\dagger$ and $\psi_{\mathbf{r}\sigma}^\dagger$ by first inverting Eqs. 2 and 3 to find:

$$a_{\mathbf{r}\sigma}^\dagger = \sum_{\mathbf{r}'} W_{\mathbf{r}-\mathbf{r}'} \phi_{\mathbf{r}'\sigma}^\dagger + w_{\mathbf{r}-\mathbf{r}'} \psi_{\mathbf{r}'\sigma}^\dagger \quad (4)$$

with $W_{\mathbf{r}} = \frac{1}{N} [\sum_{\mathbf{k} \in \mathbf{K}^>} e^{i\mathbf{k} \cdot \mathbf{r}} u_{\mathbf{k}} - \sum_{\mathbf{k} \in \mathbf{K}^<} e^{i\mathbf{k} \cdot \mathbf{r}} v_{\mathbf{k}}]$ and $w_{\mathbf{r}} = \frac{1}{N} [-\sum_{\mathbf{k} \in \mathbf{K}^>} e^{i\mathbf{k} \cdot \mathbf{r}} v_{\mathbf{k}} + \sum_{\mathbf{k} \in \mathbf{K}^<} e^{i\mathbf{k} \cdot \mathbf{r}} u_{\mathbf{k}}]$. However, because the ϕ orbitals have predominantly a character, while the ψ orbitals have predominantly b character, $a_{\mathbf{r}\sigma}^\dagger \approx \sum_{\mathbf{r}'} W_{\mathbf{r}-\mathbf{r}'} \phi_{\mathbf{r}'\sigma}^\dagger$. If $|V| \ll |t_b|$, then $|w_{\mathbf{r}}| \ll |W_{\mathbf{r}}|$. Consequently, the a subspace becomes invariant under the application of H . In addition, because $|W_0| \gg |W_{\mathbf{r} \neq 0}|$, we can establish a hierarchy of terms where the lowest order one corresponds to a simple on-site repulsion:

$$H_{eff}^U = \tilde{U} \sum_{\mathbf{r}} n_{\mathbf{r}\uparrow}^\phi n_{\mathbf{r}\downarrow}^\phi \quad (5)$$

with $\tilde{U} = U|W_0|^4$ and $n_{\mathbf{r}\sigma}^\phi = \phi_{\mathbf{r},\sigma}^\dagger \phi_{\mathbf{r},\sigma}$. The next order terms, containing three and two W_0 factors, are much smaller and are essentially the same as the intersite interactions which in the past were added to the Hubbard model to enhance the ferromagnetism [1]. Adding H_{eff}^U to H_0 we get the effective Hamiltonian:

$$H_{eff} = \sum_{\mathbf{r}, \mathbf{r}', \sigma} (\tau_{\mathbf{r}-\mathbf{r}'}^\psi \psi_{\mathbf{r}\sigma}^\dagger \psi_{\mathbf{r}'\sigma} + \tau_{\mathbf{r}-\mathbf{r}'}^\phi \phi_{\mathbf{r}\sigma}^\dagger \phi_{\mathbf{r}'\sigma}) + \tilde{U} \sum_{\mathbf{r}} n_{\mathbf{r}\uparrow}^\phi n_{\mathbf{r}\downarrow}^\phi \quad (6)$$

The ψ and ϕ orbitals form uncorrelated and correlated non-hybridized bands: $H_{eff} = H^\psi + H^\phi$. For the ϕ orbitals we obtain an effective one band Hubbard model with the peculiar double shell like dispersion relation shown by the thick lines in Fig. 1.

Particularly for $t_a = 0$, H^ϕ has a very large density of states in the lower shell of the ϕ band [1] which is located near ϵ_a . From Fig. 1 it is also clear that the electrons first doubly occupy the uncorrelated ψ band states which are below ϵ_a . However, when E_F gets close to ϵ_a , i.e. the system is in the mixed valence regime, the electrons close to the Fermi level go into some of the correlated ϕ states. Then, the interaction term H_{eff}^U , combined with the double shell band structure of H_0^ϕ , gives rise to a FM ground state (GS): The electrons close to E_F spread to higher unoccupied \mathbf{k} states and polarize, which causes the spatial part of their wave function to become antisymmetric, eliminating double occupancy in real space and reducing the Coulomb repulsion to zero. The cost of polarizing is just an increase in the kinetic energy proportional to $\delta_a \sim \hbar v_F \delta_k$, where v_F is the Fermi velocity and δ_k is the interval in \mathbf{k} space in which the electrons are polarized.

To determine the stability of this unsaturated FM state, we compare its energy with that of the PM (non-magnetic) state. If we were to build a nonmagnetic state with only the states of the lower ϕ shell, we would find a restricted delocalization for each electron because of the exclusion of the finite set of band states (\mathbf{k} -states) in the upper shell. To avoid the Coulomb repulsion U for double occupying a given site, the electrons need to occupy all \mathbf{k} -states. This means they have to occupy the ϕ states in the upper and lower shells. This restricted delocalization is a direct consequence of Heisenberg's uncertainty principle, and the resulting localization length

depends on the wave vectors, where the original b and a bands crossed, that define the size ($\Delta\mathbf{k}$) of each shell. The energy cost for occupying the ϕ states in the upper shell is proportional to the hybridization gap Δ . Therefore if U is the dominant energy scale in the problem and $\Delta \gg \delta_a$, the FM state lies lower in energy than the non-magnetic state. Under these conditions, the effective FM interaction is proportional to the hybridization gap Δ .

This mechanism for ferromagnetism on a lattice is analogous to intra-atomic Hund's mechanism polarizing of electrons in atoms. In atoms, we also have different degenerate (the equivalent of δ_a is zero) shells separated by an energy gap. If the valence shell is open, the electrons polarize to avoid the short range part of the Coulomb repulsion (again reflecting the Pauli exclusion principle). The energy of an eventual nonmagnetic state is proportional either to the magnitude of the Coulomb repulsion or to the energy gap between different shells. The interplay between both energies set the scale of Hund's intra-atomic exchange coupling.

The FM mechanism just described applies to any finite dimension. For a chain of 16 sites we calculated, by the Lanczos method, the exact GS of H_{eff} for $\epsilon_a = -t_b$, infinite \tilde{U} ($\tilde{U} \gg |\tau_F^\phi|$), and different values of V as a function of electron concentration $n = N_e/4N$. We found that the GS is a nonsaturated ferromagnet between $n = 1/4$ (one electron per site in the PAM) and $n = 3/8$. In the local momentum regime QMC [12] and DMRG [13] calculations report a FM phase in a very similar range of n , in contrast to the much broader range found by dynamical mean field theory calculations [14]. The largest magnetization M is obtained when n is such that the lower shell of the ϕ band is completely filled and the upper one is nearly empty; i.e., when $E_F \simeq \epsilon_a$.

In Fig. 2a we plot the PAM's energy per site E/N , computed by our QMC method [12], as a function of the total spin per site S/N for chains of varying length N and fixed electron density n [15]. Over these chain lengths the data collapse, with $E(S)/N$ showing the minimum E_{GS}/N at a non-zero value of S/N that represents a very good estimate of the magnetization M/N for the PAM in the thermodynamic limit (TL). In Figs. 2b and 2c, we show $\Delta E/N \equiv (E_{GS} - E(S=0))/N$ and M/N for one and two dimensional systems as a function of $1/N$. In both cases M/N smoothly varies to non-zero values in the TL. The non-smooth variation of $\Delta E/N$ in two dimensions is a consequence of shell effects still present in a finite sized system, but is clearly suggestive of its likely extrapolation to a non-negative value for very large N . In Fig. 2d we plot our QMC results for $(E(FM) - E(0))/E(0)$ as a function of ϵ_f for a 8×8 cluster and two different electron densities. As we increase ϵ_a (starting from below the bottom of the b -band) ΔE decreases and then increases. The most stable FM state occurs when $E_F \approx \epsilon_a$ as expected from our discussion of the effective model. Increasing ϵ_a even further, ΔE approaches zero indicating that the spin of the GS decreases

(see Fig. 2e) and the system becomes a paramagnet.

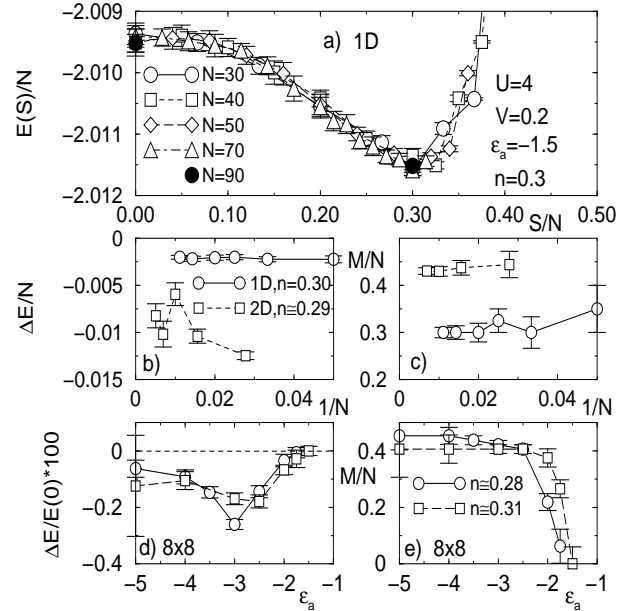


FIG. 2. a) Energy of the PAM as a function of total spin for different chain lengths. b) Scaling of the energy difference between the FM and the PM GS's of the PAM in 1D (same parameters as in Fig. 2a) and 2D ($V = 0.5$, $\epsilon_a = -0.3$, and $U = 4$). c) Scaling of the GS magnetization, otherwise, the same as b). d) Relative energy difference $\Delta E/E(0)$ vs. ϵ_a for $V = 0.5t_b$, $t_a = 0$, and $V = 0.5$, $U = 4$ and $n = 0.29$ (circles), $n = 0.31$ (squares). e) Magnetization as a function of ϵ_a for 2D, otherwise, the same as d).

By changing ϵ_a we can evolve the system from the localized ($\epsilon_a \ll E_F$) to the itinerant case ($\epsilon_a \approx E_F$). From Figs. 2d and 2e we see that the itinerant and the localized FM phases are apparently continuously connected. With decreasing ϵ_a , $|\Delta E|$ decreases while the zero temperature magnetization M increases. The strong reduction of $|\Delta E|$ is a result of the very small effective magnetic interaction in the localized limit (J_{RKKY} is order V^4 [18]). Decreasing ϵ_a increases the population of the lower ϕ -shell. Since most of the electrons in the lower ϕ shell are polarized when $\epsilon_a \leq E_F$, this leads to an increase of M . These results are consistent with the observed behavior of M and the Curie temperature T_c in $\text{La}_x\text{Ce}_{1-x}\text{Rh}_3\text{B}_2$ as function of x [19].

Even though we cannot do finite temperature calculations with our present version of the QMC method, we can discuss, at least qualitatively, the predictions of our mechanism for finite temperatures. If we move ϵ_a above E_F , the number of a -electrons decreases together with the magnetization M . A new energy scale $\epsilon_a - E_F$ emerges. We propose that this scale is responsible for the finite temperature peak in the magnetization of $\text{Ce}(\text{Rh}_{1-x}\text{Ru}_x)_3\text{B}_2$ [16] that suggests an ordered state with high entropy. At $T = 0$, M is small because of the reduced number of a -electrons. When the temperature is of the order of $\epsilon_a - E_F$, electrons are promoted from the doubly occupied b states to the unoccupied a

states which have a large entropy (large density of states). These a -electrons polarize because of the energy considerations discussed above. The source of the large entropy is thus associated with charge and not with spin degrees of freedom, which explains why a state with larger M has a higher entropy. From this analysis we predict that the entropy below T_c contains a considerable contribution from the *the charge* degrees of freedom.

We can also connect our mechanism with the hydrostatic pressure dependence of T_c . To do this we calculated $|\Delta E|/N$ by the QMC method as function of increasing t_b (Fig. 3a). Here we are assuming that the main effect of the hydrostatic pressure is to increase t_b and to leave the other parameters unchanged. The order of magnitude of $|\Delta E|/N$, which should be proportional to T_c , and its qualitative behavior in Fig. 3a are in good agreement with the experimental results in CeRh_3B_2 [11]. We see from Fig. 3a that for the itinerant FM case, $|\Delta E|/N$ is of the order of 100°K. This scale is much larger than the magnitude of the RKKY interaction [17] ($\sim 1^\circ\text{K}$) which is commonly used to explain the origin of the magnetic phase when the a electrons are localized. We also find that the FM state appears close to quarter filling and disappears for n close to $3/8$.

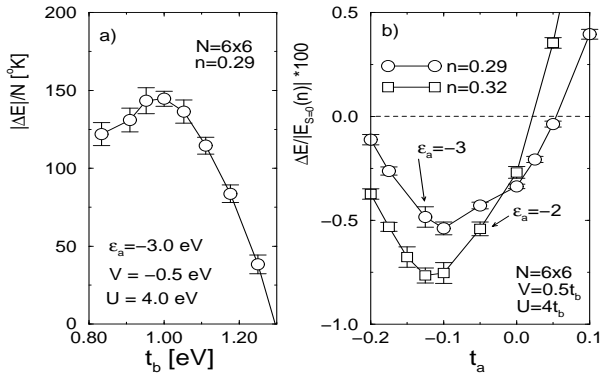


FIG. 3. a) Energy difference per site between the FM and PM states as a function of t_b . b) Influence of the hopping t_a on the FM state. The lattice size is in unit cells.

We used a nonzero t_a to study the stability of the FM phase when δ_a is varied. This study is also important because, in contrast to f electron compounds, in the FM transition metals both bands are dispersive. In Fig. 3b we see that the FM phase is even more stable for $t_a \sim -0.1t_b$ than for $t_a = 0$ and becomes unstable for $t_a \sim 0.05t_b$. The reason for this asymmetric behavior is easy to understand in terms of the variation of δ_a : If t_a is negative, then the effect of t_a on the dispersion of the ϕ band is opposite to that of the hybridization V . When $t_a \sim -0.1t_b$ we get, for the given ϵ_a and V , the minimum value for δ_a and therefore the most stable FM case. When we depart from this value of t_a , δ_a increases, $|\Delta E|$ decreases, and the FM state becomes less stable.

In summary, we introduced a novel mechanism for itinerant ferromagnetism which is present in a simple two band model. The picture just presented, combined with

our previous results [18], allows a reconciliation of the localized and delocalized ferromagnetism pictures painted by Heisenberg [3] and Bloch [4]. The hybridization between bands plays a crucial role. We have also considered the case relevant for the iron group where the dispersion of the lower band is not negligible. The fact that the ferromagnetism is even more stable for finite values of t_a indicates that our mechanism is relevant to explain the ferromagnetism of the transition metals, like Ni, where a correlated and narrow $3d$ band is hybridized with the $4s$ band. It suggests that the ferromagnetism in the transition metals can originate, at least in part, in the interplay between the correlations and the particular band structure, and not solely in the intra-atomic Hund's exchange [10]. In addition, our results explain several qualitative features observed in the ferromagnet CeRh_3B_2 [11,16,19]. Elsewhere we will discuss the relation of our mechanism to $\text{RE}(\text{Co}_{1-x}\text{Si}_x)_2$ ($\text{RE}=\text{Ho}, \text{Er}$) and the uranium monochalcogenides ($\text{US}, \text{USE}, \text{and UTe}$) which are ferromagnets [20].

Acknowledgements. This work was sponsored by the US DOE. We acknowledge useful discussions with A. J. Arko, B. Brandow, J. J. Joyce, J. M. Lawrence, S. Trugman, G. Ortiz, and J. L. Smith. We thank J. M. Lawrence for pointing out the experimental work on the Ce compounds. J. B. acknowledges the support Slovene Ministry of Education Science and Sports and FERLIN.

-
- [1] D. Vollhardt *et. al.*, Adv. in Solid State Phys. **38**, 383 (1999); Z. Phys. **B 103**, 283 (1997).
 - [2] P. Fazekas, Phil. Mag. **B 76**, 797 (1997).
 - [3] W. Heisenberg, Z. Physik **49**, 619 (1928).
 - [4] F. Bloch, Z. Physik **57**, 545 (1929).
 - [5] J. Hubbard, Proc. Roy. Soc., **A 266**, 238 (1963).
 - [6] Y. Nagaoka, Phys. Rev. **147**, 392 (1966).
 - [7] E. Lieb, Phys. Rev. Lett. **62**, 1201 (1988).
 - [8] R. Hlubina, *et. al.*, Phys. Rev. Lett. **78**, 1343 (1997).
 - [9] J. C. Slater, Phys. Rev. **49**, 537 (1936).
 - [10] J. H. van Vleck, Rev. Mod. Phys. **25**, 220 (1953).
 - [11] A. L. Cornelius, *et. al.*, Phys. Rev. B **49**, 3955 (1994).
 - [12] S. Zhang *et. al.*, Phys. Rev. Lett., **74**, 3652 (1995).
 - [13] M. Guerrero and M. N. Noack, Phys. Rev. B **53**, 3707 (1996).
 - [14] D. Meyer and W. Nolting, Phys. Rev. B **62**, 5657 (2000).
 - [15] In 1D n is unchanged as N is varied. In 2D, n changes slightly as N is varied: $n \sim 0.29$ corresponds to $N_e = 42, 74, 116, 168, 228$ as N is varied in Figs. 2b and 2c.
 - [16] S. K. Malik *et. al.*, Phys. Rev. B **31**, 4728 (1985); St. Berger *et. al.*, Phys. Rev. B, in press.
 - [17] P.-G. de Gennes, Comm. Energie At. (France) Rappt. **925**, (1959).
 - [18] C. D. Batista *et. al.*, Phys. Rev. B, **63**, 184428 (2001).
 - [19] S. A. Shaheen *et. al.*, Phys. Rev. B **31**, 656 (1985).
 - [20] P. Santini *et. al.*, Advan. in Phys. **48**, 537 (1999).